The suitability of prehistoric anthropogenic burnt sediments (*fumiers*) for archaeomagnetic studies at El Mirador cave

Ángela Herrejón-Lagunilla, Ángel Carrancho and Juan José Villalaín

Abstract

The analysis of the magnetic record of burnt archaeological materials provides valuable information of both chronological and geophysical interest. Archaeomagnetic studies carried out on independently well-dated materials allow to obtain data in order to improve and temporally extend the reference curves of the variations of the Earth's magnetic field (EMF) at regional scale (the phenomenon called "secular variation", SV). These curves, which mainly cover the last 2-3 millennia, can be used to carry out the archaeomagnetic dating. Recent research on combustion episodes from mid-late Holocene European anthropogenic cave sequences (*cf*. *fumiers*) has revealed their suitability to obtain new directional data for temporal periods poorly covered in the reference SV curves or geomagnetic field models. El Mirador cave is an ideal site for this aim. Here we present the archaeomagnetic study of 5 Holocene combustion episodes from El Mirador cave. Sampling technique is discussed and the new directional results along with a comprehensive study of their magnetic properties are assessed in connection with the previous published data. Furthermore, potential and limits of these materials to improve

Á. Herrejón-Lagunilla(*),
Departamento de Física, Universidad de Burgos,
Burgos, Spain
Departamento de Física de la Tierra y Astrofísica, Facultad de Ciencias Físicas, Universidad Complutense de Madrid;
Madrid, Spain
e-mail: aherrejon@ubu.es; anherrej@ucm.es; angelaherrejonlagunilla@gmail.com

J. J. Villalaín
Departamento de Física, Universidad de Burgos,
Burgos, Spain.
e-mail: villa@ubu.es

Á. Carrancho
Área de Prehistoria, Departamento de Historia, Geografía y Comunicación, Universidad de Burgos
Burgos, Spain.
e-mail: acarrancho@ubu.es

*Corresponding author: Ángela Herrejón-Lagunilla e-mail: angelaherrejonlagunilla@gmail.com

the archaeomagnetic dating technique for the Recent Prehistory are also discussed.

1 Introduction and state of art

The Earth's magnetic field (EMF) experiments several spatial-temporal changes at different time scales. These changes result in variations of intensity and direction of the magnetic vector. One of these changes happens at global scale as polarity inversions, where the Earth´s dipole roughly flips 180º in a matter of a few thousand years. The last polarity reversal was the Matuyama-Brunhes boundary (*ca*. 780 kyrs BP; e.g., Gradstein et al., 2004) and it has been recognized worldwide. The identification of these polarity reversals in stratigraphic sequences is a powerful correlation method as it provides additional chrono-stratigraphic markers in archaeo-paleontological sequences of at least Lower Pleistocene age. Other type of changes that the EMF undergoes take place at regional scale and on a shorter timescale. These changes are known as "secular variation" (henceforth, SV). For the purpose of this chapter, we will focus on this one.

Burnt archaeological materials such as hearths, kilns or burnt floors usually contain ferromagnetic (*s.l.*) minerals, mainly iron oxides, like magnetite or hematite. These minerals act like little compasses: their magnetic moments point to the magnetic North when heated at high temperatures (> 500 – 600 ºC) and subsequently cooled down to room temperature. This mechanism of magnetization is known as thermal remanent magnetization or thermoremanence (TRM). This TRM is a snapshot reading of the field and can be very stable upon time. Under the proviso that the material preserves its position at the moment it was last heated and cooled (*in situ, s.s.*) the EMF direction can be retrieved. The intensity, however, does not necessarily require knowing the original position of the object, but its determination is not straightforward for various methodological reasons (see, e.g., Tauxe, 2010). Since most burnt archaeological materials can be dated independently, the direction and/or intensity of the EMF at a specific moment in time can be determined. Compilation of new data from different moments allows to reconstruct the variations of the EMF in the past by the development of secular

variation (SV) curves and regional/global paleomagnetic field models. Apart from their geophysical interest, these curves and models have chronological applications, which is interesting from the archaeological viewpoint. They are the basis for the archaeomagnetic dating. By comparing the direction and/or intensity recorded on a burnt archaeological material with the available paleomagnetic models or SV reference curves, it is possible to infer the most probable date when that record took place (that is, the last heating of the material).

An important feature of the SV is that its pattern is reproducible at regional (subcontinental) scale, covering areas of no more than 600 km of radius (Lanos et al., 1999). Therefore, it is necessary to have enough data for the reconstruction of the curve for the region in which the dating is going to be performed. In the case of the Iberian Peninsula, SV behavior is well constrained up to ~1,000 yrs BCE (Gómez-Paccard et al., 2006; Molina-Cardín et al, 2018; Osete et al., 2020), both including directional and intensity data. However, there is an important lack of data before this date. Carrancho et al. (2013) carried out the archaeomagnetic study of burnt anthropogenic cave sediments in Spain spanning from ca. 5,500 to 1,000 yrs BCE and published the first directional Neolithic European paleosecular variation curve. However, there are still significant data gaps in the curve that need to be filled in order to better constrain the EMF variations. Moreover, most input data comes from Eastern Europe (mainly Bulgaria and Ukraine), with the exception of 26 new directions from three Iberian archaeological caves. Although SV trends should be relatively similar despite the geographical distance, specific patterns for Western Europe (and specifically for Iberia) could be unnoticed due to the absence of data from this area. Something similar happens to the regional/global models like the SHA.DIF.14k (Pavón-Carrasco et al., 2014), which use almost the same source of data, although it is true that improvements are being progressively made with new models (Pavón-Carrasco et al., 2021). Nowadays, according to GEOMAGIA database (https://geomagia.gfz-potsdam.de/, Brown et al., 2015); there are only 29 available archaeomagnetic directions from the Iberian Peninsula between 1,000 yrs BCE and 6,000 yrs BCE. Addition of new directional data will allow to improve and extend back in

time the Iberian SV reference curve. In this way, archaeomagnetic dating here will be significantly improved, reducing dating uncertainty prior to 1,000 yrs BCE.

One of the reasons why there is a notable paucity of prehistoric archaeomagnetic data is the difficulty in studying ancient materials, independently well-dated and carrying reliable EMF records. Volcanic flows usually carry stable magnetic signals, but they are geographically very localized and temporarily discontinuous. Previous research has shown that burnt anthropogenic cave sediments of Holocene age (*cf. fumier*s) are potential good recorders of the direction of the EMF (Carrancho et al., 2009, 2012, 2013, 2016; Kapper et al., 2014a, 2014b). *Fumier* sequences are anthropic deposits linked to the stacking and periodical burning of animal dung and plant remains in rock shelters or caves used as sheepfolds (Brochier et al., 1992; Angelucci et al., 2009; Vergès et al., 2016a). In order to reduce the volume of dung accumulated and/or clean these sites from parasites, the residues were recurrently burnt. *Fumiers´* sequences exhibit a characteristic stratigraphy where burning episodes (ashes on top of black carbonaceous facies) alternate with unburnt sediments. These contexts have been mostly studied from the archaeobotanical perspective (e.g.: Alonso-Eguíluz et al., 2016; Cabanes et al., 2009; Elliot et al., 2014) and more recently, zooarchaeological and isotopic (e.g.: Martín et al., 2016, 2021), geochemical (Gea et al., 2017) and geoarchaeological analyses have also been carried out (e.g.: Polo et al., 2014, 2016). Their wide geographic and chronological distribution, good preservation and availability of accurate dates (mainly ^{14}C) make them excellent candidates for obtaining archaeomagnetic data. Surprisingly, however, very few archaeomagnetic studies in this type of sites have been carried out so far.

As discussed later, as long as these materials meet certain requirements, they are good candidates to improve and extend regional SV curves and paleomagnetic models. Many of the existing prehistoric archaeomagnetic data in Iberia comes from previous studies at El Mirador cave (Carrancho et al., 2009, 2012, 2013, 2016). The good preservation conditions of its burning episodes, its exceptional chronological control as well as its meticulous

excavation and recording process were key to generate the aforementioned directional European paleosecular variation curve (Carrancho et al., 2013).

Apart from this geophysical interest, archaeomagnetic data also provide twofold archaeological information. Firstly, the progressive thermal demagnetization of the natural remanent magnetization (NRM) may reveal the last heating temperature experienced by the material. Indirectly, the analysis of the reversibility of thermomagnetic curves may also provide that information. This is interesting not only to reconstruct the technological abilities of these human groups in the past but also to evaluate the preservation of certain organic components in the sediment such as phytoliths or other paleobotanical remains. Secondly, the sensitivity of archaeomagnetic analyses to identify mechanical (physical) disturbances on combustion episodes makes this technique a versatile tool for assessing their preservation at microscopic scale (Carrancho et al., 2012). As will be seen later, this has important archaeological and even geochronological implications. This study aims to explore also the archaeological applications of the archaeomagnetic method.

Bearing all this in mind, here we report an archaeomagnetic study on 5 new burning episodes from Sector 100 of El Mirador cave. Both archaeological and geophysical implications of the method are discussed, with particular emphasis on the assessment of post-depositional and formation processes and the integrity of the archaeological record. In addition, potential and limits of archaeomagnetism in these archaeological contexts are discussed.

2 Materials and Methods

An archaeomagnetic study of five combustion episodes (Ci2, Ci3, Ci5, Ci6 and Ci7; Supplementary Information 1, 2 and 3) from Sector 100 of El Mirador cave has been carried out (Vergès et al., this book). Ci2 and Ci3 correspond to level MIR104. The dating of MIR104 performed on a charcoal yields an age interval of 1,710-1,510 cal yrs BCE (2σ; 3,350±30 yrs BP) (Vergès et al., 2016a). Combustion episode Ci2 is located just above Ci3, in direct contact (Supplementary Information 2). Ashes (*s.l.*) from these episodes reach a great thickness (up to 20-25 cm approximately; Supplementary Information 2).

Occasionally, small (centimeters-sized) irregular limestone blocks were observed within the ashes. The underlying dark colored carbonaceous facies is around 2 cm of thickness. Both facies (ashes and underlying carbonaceous facies) are interpreted as the result of the same combustion event and this has been tested experimentally (Vergès et al., 2016b).

Burning episodes Ci5, Ci6 and Ci7 are included in level MIR107. They are stratigraphically below Ci2 and Ci3, separated from them by around 150 cm. Ci5 event is the uppermost of the studied episodes from level MIR107 (Supplementary Information 3). Ci6 is below Ci5 and Ci7 is the deepest episode from the studied series (Supplementary Information 3). Each combustion episode is composed of an ash layer on top and an underlying carbonaceous facies. Their regular geometry and the lateral continuity of the facies is, in principle, indicative that these events can preserve their primary position. Age of level MIR107 is constrained by a radiocarbon dating on a charcoal (*Quercus* sp.) between 4,542 and 4,371 cal yrs BCE [95.4% of probability, using INTCAL13 (Reimer et al., 2013); 5,640 ±30 yrs BP] (Vergès et al., this book).

Sampling was performed through the stratigraphic profiles, using a specific device designed for soft (non-lithified) materials. It specifically consists of a nonmagnetic cylindrical piston, which is carefully pressed against the vertical profiles where the burning features are exposed in section and includes a built-in orientation system (Supplementary Information 4; Carrancho et al., 2013). Sampled materials were mainly ashes, although some underlying carbonaceous samples were also collected (Supplementary Information 1 and 5). A total of 127 oriented specimens were collected in cylindrical plastic or quartz capsules (Ø 16.5 mm, length 17 mm, and vol. ~3.6 cm^3) in order to obtain directional data. The specimens were introduced in quartz or plastic capsules depending on whether they were to be thermally demagnetized or by alternating fields, respectively. Some of the specimens encapsulated in quartz capsules were previously consolidated with a mixture of Sodium Silicate and water.

The natural remanent magnetization (NRM) of 21 specimens was thermally (TH) demagnetized (15-19 steps up to 580-625 ºC). This procedure was carried out with a 755 Superconducting Rock Magnetometer (2G) and a TD48-DC oven

(ASC). The remaining specimens (106) were analyzed by alternating field (AF) demagnetization in 18 to 21 steps up to 80-100 mT. An AF demagnetization unit coupled to the magnetometer was used for this aim. The direction of the characteristic remanent magnetization (ChRM) of all specimens was determined by principal component analysis (Kirschvink, 1980) and their statistical parameters were calculated following Fisher (1953) statistics. The *Remasoft* software (Chadima and Hrouda, 2006) was used to analyze the palaeomagnetic results. Initial magnetic susceptibility at room temperature was measured in most of the oriented specimens, using a Kappabridge KLY-4 (AGICO).

Bulk samples from representative facies were also collected for rock-magnetic analyses. They consisted of progressive acquisition of the isothermal remanent magnetization (IRM) curves, hysteresis loops (± 1 T), backfield coercivity curves and thermomagnetic curves (temperature *vs.* magnetization). A variable field translation balance (Magnetic Measurements) was used to perform these experiments on powdered samples (~150-300 mg). The results were interpreted with the aid of the *RockMag Analyzer* software (Leonhardt 2006).

All these analyses were carried out in the Paleomagnetism Laboratory of the University of Burgos, Spain.

3 Results

3.1 Magnetic properties

NRM values range between 9.1 x 10^{-6} and 9.1 x 10^{-4} Am^2kg^{-1}. Magnetic susceptibility (at room temperature) oscillates between 6.4 x 10^{-8} and 4.4 x 10^{-6} m^3kg^{-1} (Supplementary Information 5). NRM and susceptibility values of ashes tend to be higher than those of the carbonaceous facies. Königsberger ratio or Q_n ratio (Stacey, 1967), which is a parameter commonly used in the study of burnt materials to assess if the material carries a stable TRM signal, is ≥1 in most cases, ranging between 0.72 and 8.2 (Supplementary Information 5). Progressive IRM acquisition curves show the dominance of low coercivity materials (Fig. 1a). Magnetite is the main ferromagnetic mineral observed in the thermomagnetic curves, with Curie temperatures (T_C) around 580 ºC (Fig. 1b-

g). Frequently, the T_C is a little bit higher than 580 ºC (~600-610 ºC), which suggests that the magnetite is slightly oxidized (e.g., Fig. 1b-d). In some cases, a drop around 300 ºC is detected both in heating and cooling curves (Fig. 1e). It might be indicative of the presence of magnetite with an important content of substituents cations (Ti, Al, Mg). Interestingly, the high degree of reversibility observed in ashes (coincidence between the heating and cooling cycles) is indicative that they underwent high temperatures (> 700 ºC) in the past. This is the case of Figures 1b-e. In some cases, a bump around 200 ºC was observed during the heating (Fig. 1c-d). A similar behavior has been observed in other archaeological burnt materials (Bradák et al., 2021, Herrejón Lagunilla et al., 2021). Regarding the hysteresis ratios, M_{RS}/M_S oscillates between 0.08 and 0.18 whereas the ratio B_{CR}/B_C varies between 2.21 and 4.08. Hysteresis ratios yield information about the magnetic domain-state (granulometry) of the samples, which in turn, is also related with the stability of the magnetization. Both ashes and carbonaceous samples lie in the pseudo-single domain (PSD) region of that biparametric ratio also known as the “Day et al. (1977) plot” (Supplementary Information 6). In general terms, all the samples fall in the same area of the plot, although some ashes tend to be closer to the multidomain (MD) area (further down and further to the right in the graph).

Fig.1 a. Progressive isothermal remanent magnetization acquisition curves (IRM); **b-g.** thermomagnetic curves (temperature vs. induced magnetization) of ashes and carbonaceous facies. Heating (cooling) cycles are shown in red (blue). Sample code and type of facies are also shown

3.2 Paleomagnetic analyses: new directions from El Mirador cave

Depending on the type of facies analyzed and their NRM structure, two different types of magnetic behavior have been distinguished as described in the following. All samples studied display a secondary component of viscous origin easily removed < 15 mT in the AF demagnetized specimens and < 150 – 250 ºC in the thermally demagnetized ones. Although we have not carried out a viscous remanent magnetization (VRM) study here, we have the reference of a previous study on these types of materials. Carrancho et al. (2009) carried out a VRM acquisition experiment in four Neolithic *fumiers* from El Mirador cave determining a mean viscosity index of around 12% in the ashes and almost 20% in the carbonaceous facies. Our main purpose in the lab is to isolate the

ChRM direction. That is, the Earth's magnetic field direction recorded in the last heating. This magnetic behavior has been already observed on this type of materials by Carrancho et al. (2009, 2013, 2016).

In order to select the specimens for the calculation of the ChRM mean direction, the following quality criteria have been considered:

1) Specimens with Köenigsberger (Q_n) ratio values < 1 were disregarded, following the criteria of Carrancho et al. (2013). That is an indication that the magnetization is not an undisturbed TRM.

2) According to the high degree of reversibility observed in the thermomagnetic curves, ashes reached high temperatures (>600 - 700 °C), higher than the Curie temperature of the main carrier of the magnetization: magnetite, T_C ~580 ºC (Dunlop and Özdemir, 1997). Therefore, only specimens with univectoral demagnetization diagrams (excluding the viscous component) were accepted for this facies. (Fig. 2a-b). This criterion was also suggested by Carrancho et al. (2013). It was not applied to the subjacent carbonaceous facies, since it is expected that they reached lower temperatures than ashes. The irreversibility of their thermomagnetic curves (Fig. 1f-g) and the identification of partial thermoremanences (p-TRMs) in their orthogonal NRM demagnetization diagrams are indicative that they did not exceed 450 ºC (Fig. 2c). This also agrees with our previous paleotemperature experiments performed in the carbonaceous facies of *fumiers* (e.g.: Carrancho et al., 2016).

Fig. 2 Orthogonal NRM demagnetization plots of five representative specimens (ashes and carbonaceous facies) from the burning events studied: **a & e**. AF demagnetized diagrams; **b-d.** Thermal demagnetization plots. Solid/open circles in orthogonal plots represent the projections of vector endpoints onto the horizontal/vertical plane. The initial intensity (NRM), sample code, facies, main demagnetization steps and the normalized demagnetization intensity spectra are shown for each specimen

3) Specimens in which the ChRM direction could not be identified and/or isolated due to the presence of overlapping magnetic components (vectors) or unstable behaviors have been excluded (e.g., Fig. 2d-e).

4) Once the previous criteria were applied, specimens with an angular distance from the mean direction greater than 3 x α95 were disregarded. Similar criteria

were used in previous studies of analogous materials (Kapper et al., 2014a, 2014b).

For the final selection of specimens, the calculation of the ChRM direction was carried out considering the type of facies analyzed (ashes and carbonaceous facies) and their NRM structure, which is reproducible for all the five events studied. The ashes are characterized by an intense, well-defined normal polarity magnetic component between 15-35 mT and 80-100 mT (AF demagnetization) (Comp. A in Fig. 2a). The ashes thermally demagnetized defined their ChRM direction between 250 ºC and 550–600 ºC (Comp. A in Fig. 2b). In the carbonaceous facies, the ChRM direction was isolated between 20-35 mT and 100 mT in the AF specimens. The thermal demagnetization revealed the occasional presence of partial thermoremanences (pTRM) in this facies between 150-200 ºC and 350-450 ºC (e.g.: component A1 in Fig. 2c). These maximum unblocking temperatures (max T_{UB}) up 450 ºC in the carbonaceous facies indicate the maximum heating temperature reached by this facies in their last heating. This is in good agreement with the irreversibility previously described in their thermomagnetic curves (Fig. 1f-g). Finally, a high temperature component from ~475–600 ºC (comp. B in Fig. 2c) is observed in the carbonaceous specimens thermally cleaned, which can be interpreted as the original magnetization of the substrate. This component has normal polarity.

Five mean archaeomagnetic directions have been obtained. Their equal area projections along with their Fisher´s (1953) statistical associated data are shown in Figure 3. The mean directions are calculated with a minimum of 10 specimens per feature, the dispersion parameter (*k*) is reasonably acceptable ranging from 22 to 78 and the α95 is in all cases but one lower than 8.3º.

Fig. 3 Equal area projection of the five new mean archaeomagnetic directions from El Mirador cave and their associated statistical parameters according to Fisher (1953). N = specimens considered for the calculation of the mean direction; N' = total number of demagnetized specimens; Dec. = declination; Inc. = inclination; α95 = semi angle of confidence at 95% of probability; *k* = precision parameter. Solid/open symbols correspond to downward/upward inclination

4 Discussion

4.1 Comparison with previous published data and new directions

The new archaeomagnetic data exhibit quality levels similar to those from previous published archaeomagnetic directions from El Mirador cave (Carrancho et al., 2013, 2016) as well as similar materials in other European caves (Carrancho and Villalaín, 2012; Kapper et al., 2014a, 2014b). An indicator of the quality of the directions is the precision parameter, *k*. The lower *k*, the less clustering of the directions of the specimens considered for the mean calculation. In other words, the dispersion will increase and theoretically, this should not be the case in an *in situ* (*s.s.*), well-heated material (e.g.: Carrancho et al. 2012). Our new directions range between 21.9 and 78.2 (median = 34.7). In the combustion episodes from the Holocene levels of El Mirón cave (Cantabria, Spain), El Mirador cave and El Portalón cave (Sierra de Atapuerca, Burgos, Spain) studied by Carrancho et al. (2013), *k* values range between 17.2 and 211.3 (median = 91.2). In the specific case of El Mirador cave's archaeomagnetic directions (from 15 combustion episodes), their *k* values range between 38 and 211 (median = 79.5). Another archaeomagnetic direction from a combustion episode of El Mirador cave was presented by Carrancho et al. (2016), yielding a *k* = 63.3. Kapper et al. (2014b) studied similar materials in Arconciel cave (Fribourg, Switzerland) with *k* values ranging between 44.9 and 703.5 (median = 88.8). Another study with analogous materials was performed in Riparo Gaban rock shelter (Trento, Italy; Kapper et al., 2014a). Here, the *k* values of the combustion episodes accepted from the statistical point of view range between 18.3 and 63.8 (median = 32.3). Another interesting parameter with regard to the quality of the directions is α95 (the semi angle of confidence at 95% of probability). This parameter is highly dependent on the number of specimens (the greater number of specimens analyzed, the lower is the α95), but is also informative of the statistical quality of the results. The α95 values of the dataset of Carrancho et al. (2013) which included 26 directions ranges between 2.6º and 12º (between 2.6º and 8º in El Mirador cave, between 4.3º and 12º in El Mirón cave; and between 3.1º and 4.6º in El Portalón cave) and the number of specimens considered for the calculation of the mean directions (*n*) ranges between 7 and 28. The Bronze age archaeomagnetic direction reported from El Mirador cave by Carrancho et al. (2016) has an α95 = 4.4º (n = 18). Similarly, in the archaeomagnetic study of various prehistoric combustion episodes from Arconciel site (Kapper et al., 2014b), α95 values are between

2.8º and 9.8º (6 ≤ n ≤ 20). In Riparo Gaban, considering only the accepted mean directions, they oscillate between 5º and 13.3º (6 ≤ n ≤ 14) (Kapper et al., 2014a). The mean directions of the combustion episodes presented in this chapter exhibit α95 values between 3.4º and 13.2º, being four of the five ≤ 8.3º (7 ≤ n ≤ 26). It should be pointed out that a selection of the best combustion episodes (in terms of archaeomagnetic statistical results) was usually made in the cited studies. Hence, taking into account the nature of the studied materials, we can assume that our results have similar quality than those published elsewhere.

4.2 Archaeological implications of archaeomagnetic data with regard to formation processes and the integrity of the archaeological record.

The magnetic behavior of the studied facies is directly related to their formation processes. It has been previously observed that ashes (*sensu stricto*) mainly constitute the calcined (or at least, highly heated) remains of fuel, while the carbonaceous facies is the thermoaltered surface above which the fire was carried out (Polo-Díaz et al. 2016). The detection of pTRMs with maximum unblocking temperatures of 350-450 ºC along with highly irreversible thermomagnetic curves corroborates that the carbonaceous facies experimented lower temperatures than ashes. These, in contrast, exhibit highly reversible thermomagnetic curves pointing out that they reached about 600 ºC and even more. This specific issue is further discussed in the next chapter by means of the combination of different analyses and techniques that include magnetic results (Burguet-Coca et al., this book).

Besides that, archaeomagnetic analyses allow to assess the preservation of the combustion episodes and the integrity of the archaeological record. It must be noted that our research strategy at the site involved sampling every feature covering all parts and every facies potentially burnt or at least, showing signs of having undergone heating. Obviously, there may be variability in the ashes and/or carbonaceous facies in terms of facies´ thickness, physical preservation and temperatures attained. On many occasions, the macroscopical appearance of the combustion episodes is good (ashes on the top and carbonaceous facies/rubifaction on the base; lateral continuity, etc.), but internal or

microscopic mechanical disturbances cannot be noticed to the naked eye in the field. However, they can be easily detected later from the magnetic data. Archaeomagnetic analyses are very sensitive to mechanical alterations. The movement of ferromagnetic grains of the archaeosedimentary facies induced by any post-depositional process after heating generates unstable and less intense NRM diagrams, resulting in Q_n ratio values lower than 1 and a higher scatter of the archaeomagnetic directions (e.g. Carrancho et al. 2012). All these factors are indicative that the burning event has undergone some type of mechanical (physical) disturbance. Consequently, there is a clear correlation between the quality of the archaeomagnetic data obtained and the degree of preservation of the sampled features. Currently, the application of analytical techniques to explore archaeological contexts at a microscale level is gaining importance and archaeomagnetism can definitely contribute to that aim.

In general terms, our directional results are comparable to those obtained in other studies and sites (see section 4.1). However, some details deserve a comment. The scatter is greater in Ci5, Ci6 and Ci7. It could be argued that the number of specimens processed in each case marks the difference. In well-preserved episodes the number of specimens should not be particularly problematic (as long as there is a minimum number of specimens to obtain acceptable statistical parameters, which usually is no lower than 8) because all of them would be representative of the general behavior. Something similar happens in poorly preserved episodes where any area of sampling is affected by mechanical disturbances. If all areas are similarly affected, any sampled zone is representative of the general “bad” behavior. However, in episodes that have experienced reworking of only part of their structure, the number and location of samples is more critical. Depending on where the specimens are collected, we will be studying well or poorly preserved areas and that will be shown in the statistical quality of the archaeomagnetic data. A good example of this is the case presented in Carrancho et al. (2012), where a combustion episode was partially cut by a burrow. Considering this, sampling should always focus on all areas of the combustion episodes. Obviously, within the possibilities of accessibility and taking into account whether the burning event is macroscopically well preserved (e.g.: lateral continuity of its facies, absence of

bioturbation, etc.). In this way, the sampling would be as representative as possible of the whole episode. Thus, we suggest that internal (microscopic) preservation of Ci5, Ci6 and Ci7 is not optimal from the archaeomagnetic point of view, but no so problematic from the archaeological perspective. Otherwise, all samples in the stereograms would be randomly distributed with high α95 and particularly very low *k* values, and that is not the case (Fig. 3).

Some differences in preservation conditions between Ci2 and Ci3 can be also inferred. In this case, the number of collected and accepted specimens is very similar. The α_{95} value of Ci2 is comparable to that from Ci3. However, the *k* value of Ci3 is twice the value of Ci2. It indicates a greater scatter in Ci2 than Ci3. Thus, a better preservation in Ci3 than Ci2 is suggested. Although they are not statistically perfect data, they are not aberrant enough to indicate a systematic reworking or alteration of these combustion events.

Bearing in mind the aforementioned issues and also that we are dealing with non-lithified materials, the preservation at the microscopic scale is rather acceptable in the studied cases. Within its variability, no aberrant scatter is observed and all archaeomagnetic directions obtained fall within the expected range of dispersion for secular variation in mid-latitudes. If the directional results and their statistics were very poor due to severe post-depositional processes, this might compromise the archaeological record and its reliability. Nevertheless, no displacements of archaeological remains (e.g.: potteries, charcoals, bones, etc.) have been observed in this stratigraphy. More importantly, evaluating these processes also have geochronological implications. For instance, if the samples used in radiometric dating such as charcoals, seeds, or the sediment itself are not *in situ* or have undergone significant mechanical removal, the dating results may cast serious doubts or directly be wrong. Therefore, evaluating these processes is important to ensure the integrity of the record, and archeomagnetism is very useful for this.

4.3 Potential and limits of the combustion episodes from *fumiers'* sequences for archaeomagnetic purposes

Episode combustions from *fumiers* have been revealed as good recorders of the EMF direction. Furthermore, their chronologies (from Early Neolithic to Iron age; Angelucci et al., 2009) make them probably the best option to improve with detail the secular variation curve of the Iberian Peninsula up to the 6th millennia BCE. It is worth to remark that the period between 1,500 and 4,000 yrs BCE is poorly constrained in the Iberian archaeomagnetic database and, to our knowledge, no other radiometrically well-dated burnt archaeological materials are easily available for archaeomagnetic purposes. Isolated burning features can always be analyzed but the possibility of studying multiple and well-dated combustion events along continuous stratigraphic sequences is rather exceptional. Given their geographic ubiquity throughout the circum-Mediterranean area (Angelucci et al., 2009), their potential is high and deserves more attention.

However, the combustion episodes from the *fumiers´* sequences also present some problems or limitations. These materials (*fumiers*) are far from standard in archaeomagnetism for several reasons. Firstly, by the type of archaeological material. Most archaeomagnetic studies are carried out on burned materials such as kilns, walls, bricks and so on. These are all lithified materials or with a certain degree of consistency, that allows their sampling with high precision using water-cooled electrical or even gasoline drills. These sampling techniques cannot be used in *fumiers* sequences as we are dealing with soft (non-lithified) sediments. The collection and magnetic orientation of multiple specimens with the highest accuracy possible is a key aspect to obtain good results (beyond the magnetic behavior of the material itself). Not to mention that the invasiveness of the sampling method also has an impact. Our sampling strategy allows the collection of multiple specimens (usually between 10 to 15 and even more) with relatively little impact on the structure. Secondly, the preservation of burning events in *fumiers´* sequences is more complicated than in other archaeological materials. Due to their unconsolidated nature, these sediments are prone to be reworked by different factors (e.g.: trampling, animal bioturbation, etc.). From the archaeomagnetic point of view this is a problem because mechanical disturbances (event at grain scale) may distort the directional results. No matter how minimal, it will have an effect on the dispersion of the dataset (evidenced

by low values in the precision parameter *k*) or other magnetic properties. In this sense, the ratio between the accepted and analyzed specimens is meaningful. From a total 127 specimens demagnetized, only 77 have been considered for the calculation of the mean archaeomagnetic directions (~61%). This percentage is very similar to that of previous studies. For the calculation of the mean directions of 26 combustion episodes, Carrancho et al. (2013) considered reliable 338 specimens out of a total of 496 (~68%). In the case of the Bronze Age combustion episode from El Mirador cave studied by Carrancho et al. (2016), a ~62% of the measured specimens (18 from a total of 29) was finally accepted. The percentage of accepted specimens in the study of Kapper et al. (2014b) at Arconciel cave is ~65% (89 specimens out of a total of 137). In Riparo Gaban (Kapper et al., 2014a), 68 out of 107 demagnetized samples were finally considered for the mean direction calculation of the accepted combustion episodes (~63%). These data indicate that around 30-40 % of the specimens are excluded when this kind of materials are archaeomagnetically investigated. A careful observation in the field is very important in order to sample the best-preserved areas. Macroscopically, well-preserved combustion episodes should contain an ash facies of variable thickness (*ca*. 2 up to 10 cm) on top and an underlying carbonaceous and/or rubefaction facies. The color of these facies will strongly depend on the environmental conditions during burning (reducing *vs*. oxidizing). The observation of alterations like postholes or burrows is a clear indication that some type of post-depositional processes has taken place (Carrancho et al., 2012). This suggests not considering that event for archaeomagnetic purposes or at least extreme the caution in sampling trying to avoid the reworked area. Even so getting a good archaeomagnetic direction is not assured at all as Carrancho et al. (2012) demonstrated.

Finally, *fumiers* are remarkably old materials in comparison with those traditionally studied in archaeomagnetism. With some exception, most regional secular variation (SV) curves span the last 2-3 millennia (e.g., Molina-Cardín et al., 2018; Le Goff et al., 2020; Schnepp et al., 2020; Tema and Lanos, 2021). There are older data, but they are temporally isolated records and do not come from continuous and independently well-dated stratigraphic sequences like these. For this reason, despite the difficulty of obtaining archaeomagnetic

directions with acceptable statistical quality, it is important to work further in this type of contexts to extend temporally and geographically the existing archaeomagnetic databases. Undoubtedly, this will improve the resolution of the dating technique.

5 Conclusions

An archaeomagnetic study has been performed in five combustion episodes from Neolithic and Bronze Age burnt levels at El Mirador cave, obtaining five new archaeomagnetic directions. Although their statistical results are variable, all fall within the expected range of dispersion of the secular variation for mid-latitudes. These data are of similar quality to those reported in analogous studies indicating that these materials (*fumiers*) are suitable records of the ancient Earth's magnetic field. Therefore, as independent well-dated materials, they can be used for geomagnetic field modelling purposes. From the archaeological viewpoint, the archaeomagnetic directions obtained are not scattered enough as to indicate a systematic reworking or alteration of these combustion events. This indicates that these combustion events are reasonably well-preserved on a microscopic scale, which is also consistent with the absence of translocated archaeological remains in the stratigraphy. Being able to guarantee the physical integrity of combustion events like these allows us to have confidence in the radiometric dating of the material extracted from them (e.g.: charcoals, seeds). As long as the facies composing these burning events are adequately preserved (ashes overlying carbonaceous facies), without clear evidences of post-depositional alteration processes, there is a high chance of obtaining an archaeomagnetic direction.

The progressive compilation of archaeomagnetic data from these materials will allow reconstructing and extending back-in time the behavior of the EMF in the past, which is a contribution of geophysical and chronometric interest. Archaeomagnetic data from prehistoric times are scarce and particularly those before 1,500 yrs BCE. To the extent that we are able to obtain new and older archaeomagnetic data of these chronologies, the regional secular variation curves and geomagnetic field models which are currently used for archaeomagnetic dating will be improved. Some methodological

recommendations are also suggested, such as an exhaustive observation of the geometry and lateral continuity of the combustion episodes in the field and the collection of a high number of specimens to improve the statistics. Finally, we would like to highlight also the archaeological utility of magnetic analyses not only to determine ancient heating temperatures but also for assessing the primary position (*in situ, s.s.*) of these burning features and evaluating the formation and alteration processes in archaeological sites.

Acknowledgements

Authors give special thanks to Josep Maria Vergés and all the excavation team of El Mirador cave, whose work has allowed to develop the present study. Authors thank the support of the Spanish Ministry of Universities and European Union-NextGenerationEU (Margarita Salas Grants), European Social Fund (Operational Programme for Castilla y León) and the Junta de Castilla y León (Consejería de Educación). The support of the projects PID2019-107113RB-I00 / AEI / 10.13039/501100011033, PID2019-105796GB-I00 / AEI / 10.13039/501100011033 and PID2019-108753GB-C21/ AEI / 10.13039/501100011033 (financed by Agencia Estatal de Investigación, Spain) and BU235P18 (funded by Junta de Castilla y León and European Fund of Regional Development) is also appreciated by the authors.

References

Alonso-Eguíluz, M., Fernández-Eraso, J., Albert, R. (2017). The first herders in the upper Ebro basin at Los Husos II (Álava, Spain): microarchaeology applied to *fumier* deposits. *Vegetation History and Archaeobotany*, 26, 143–157. http://doi.org/10.1007/s00334-016-0590-y

Angelucci, D. E., Boschian, G., Fontanals, M., Pedrotti, A., Vergés, J. M. (2009). Shepherds and karst: The use of caves and rock-shelters in the Mediterranean region during the Neolithic. *World Archaeology*, 41(2), 191–214. https://doi.org/10.1080/00438240902843659

Bradák, B., Carrancho, Á., Herrejón Lagunilla, Á., Villalaín, J. J., Monnier, G. F., Tostevin, G., Mallol, C., Pajović, G., Baković, M., Borovinić, N. (2021). Magnetic fabric and archaeomagnetic analyses of anthropogenic ash horizons in a cave

sediment succession (Crvena Stijena site, Montenegro). *Geophysical Journal International*, 224(2), 795–812. https://doi.org/10.1093/gji/ggaa461

Brochier, J.E., Villa, P. Giacomarra, M., Tagliacozzo, A. (1992). Shepherds and sediments: geo-ethnoarchaeology of pastoral sites. *Journal of Anthropological Archaeology*, 11(1), 47–102. https://doi.org/10.1016/0278-4165(92)90010-9

Cabanes, D., Burjachs, F., Expósito, I., Rodríguez. A., Allué, E., Euba, I., Vergès, J.M. (2009). Formation processes through archaeobotanical remains: the case of the Bronze Age levels in El Mirador cave, Sierra de Atapuerca, Spain. *Quaternary International*, 193, 160–173. https://doi.org/10.1016/j.quaint.2007.08.002

Carrancho, Á., Herrejón Lagunilla, Á., Vergès, J. M. (2016). Three archaeomagnetic applications of archaeological interest to the study of burnt anthropogenic cave sediments. *Quaternary International*, 414, 244–257. https://doi.org/10.1016/J.QUAINT.2015.10.010

Carrancho, Á., Villalaín, J.J. (2012). Preliminary archaeomagnetic and rock-magnetic results from the holocene fire lenses in el Mirón cave. In: L.G. Straus, M.R. González Morales (Eds.): *El Mirón Cave, Cantabrian Spain: The Site and its Holocene Archaeological Record* (pp. 103-118). Albuquerque: University of New Mexico Press.

Carrancho, Á., Villalaín, J. J., Angelucci, D. E., Dekkers, M. J., Vallverdú, J., Vergés, J. M. (2009). Rock-magnetic analyses as a tool to investigate archaeological fired sediments: A case study of Mirador cave (Sierra de Atapuerca, Spain). *Geophysical Journal International*, 179(1), 79–96. https://doi.org/10.1111/j.1365-246X.2009.04276.x

Carrancho, A., Villalaín, J. J., Pavón-Carrasco, F. J., Osete, M. L., Straus, L. G., Vergès, J. M., Carretero, J.M., Angelucci, D.E., González Morales, M.R., Arsuaga, J.L., Bermúdez de Castro, J.M., Carbonell, E. (2013). First directional European palaeosecular variation curve for the Neolithic based on archaeomagnetic data. *Earth and Planetary Science Letters*, 380, 124–137. https://doi.org/10.1016/j.epsl.2013.08.031

Carrancho, Á., Villalaín, J. J., Vergés, J. M., Vallverdú, J. (2012). Assessing post-depositional processes in archaeological cave fires through the analysis of archaeomagnetic vectors. *Quaternary International*, 275, 14–22. https://doi.org/10.1016/j.quaint.2012.01.010

Chadima, M., Hrouda, F. (2006). Remasoft 3.0 – a user-friendly paleomagnetic data browser and analyzer. *Travaux Géophysiques*, XXVII, 20–21.

Day, R., Fuller, M., Schmidt, V. A. (1977). Hysteresis properties of titanomagnetites: Grain-size and compositional dependence. *Physics of the Earth and Planetary Interiors*, 13(4), 260–267. https://doi.org/10.1016/0031-9201(77)90108-X

Dunlop, D.J. (2002). Theory and application of the Day plot (M rs / M s versus H cr / H c) 1. Theoretical curves and tests using titanomagnetite data. *Journal of Geophysical Research*, 107(B3), 1–22. http://doi.org/10.1029/2001JB000486

Dunlop, D.J., & Özdemir, Ö. (1997). *Rock Magnetism. Fundamentals and Frontiers*. Cambridge: Cambridge University Press. http://doi.org/10.1017/CBO9780511612794

Elliott, S., Bendrey, R., Whitlam, J., Aziz, K.R., Evans, J. (2014). Preliminary ethnoarchaeological research on modern animal husbandry in Bestansur, Iraqi Kurdistan: integrating animal, plant and environmental data. *Environmental Archaeology*, 20, 238–303. http://doi.org/10.1179/1749631414Y.0000000025

Fisher, R.A. (1953). Dispersion on a sphere. *Proceedings of the Royal Society of London A217*, 295–305. https://doi.org/10.1098/rspa.1953.0064

Gea, J., Sampedro, M.C., Vallejo, A., Polo-Díaz, A., Goicolea, M.A., Fernández-Eraso, J., Barrio, R.J. (2017). Characterization of ancient lipids in prehistoric organic residues: Chemical evidence of livestock-pens in rock-shelters since Early Neolithic to Bronze age. *Journal of Separation Science* 40(23), 4549-4562. http://doi.org/ 10.1002/jssc.201700692.

Gómez-Paccard, M., Chauvin, A., Lanos, P., McIntosh, G., Osete, M. L., Catanzariti, G., Ruiz Martínez, V.C., Núñez, J.I. (2006). First archaeomagnetic

secular variation curve for the Iberian Peninsula: Comparison with other data from western Europe and with global geomagnetic field models. *Geochemistry, Geophysics, Geosystems*, 7(12). https://doi.org/10.1029/2006GC001476

Gradstein, F.M., Ogg, J.G., Smith, A.G. (2004). *Geologic Time Scale.* Cambridge: Cambridge University Press.

Herrejón Lagunilla, Á., Villalaín, J. J., Carrancho, Á., Alonso Fernández, C., Jiménez Echevarría, J., Pavón Carrasco, F. J. (2021). Dating a medieval pottery workshop of the city of Burgos (Spain): Archaeomagnetic and archaeological evidences. *Physics of the Earth and Planetary Interiors*, 316, 106723. https://doi.org/https://doi.org/10.1016/j.pepi.2021.106723

Kapper, K. L., Anesin, D., Donadini, F., Angelucci, D. E., Cavulli, F., Pedrotti, A., Hirt, A. M. (2014a). Linking site formation processes to magnetic properties. Rock- and archeomagnetic analysis of the combustion levels at Riparo Gaban (Italy). *Journal of Archaeological Science*, 41, 836–855. https://doi.org/10.1016/j.jas.2013.10.015

Kapper, K. L., Donadini, F., Mauvilly, M., Panovska, S., Hirt, A. M. (2014b). New directional archaeomagnetic data of burned cave sediments from Switzerland and geomagnetic field variations in Central Europe. *Geophysical Journal International*, 198(2), 1208–1221. https://doi.org/10.1093/gji/ggu184

Kirschvink, J.L. (1980). The least-squares line and plane and the analysis of palaeomagnetic data. *Geophysical Journal of the Royal Astronomical* Society 62, 699-718.

Lanos, P., Kovacheva, M., Chauvin, A. (1999). Archaeomagnetism, methodology and applications. Implementation and practice of the archaeomagnetic method in France and Bulgaria. *European Journal of Archaeology* 2(3), 365-392. https://10.1179/eja.1999.2.3.365

Le Goff, M., Gallet, Y., Warmé, N., Genevey, A. (2020). An updated archeomagnetic directional variation curve for France over the past two millennia, following 25 years of additional data acquisition. *Physics of the Earth*

and Planetary Interiors, 309, 106592. https://doi.org/10.1016/j.pepi.2020.106592

Leonhardt, R. (2006). Analyzing rock magnetic measurements: The RockMagAnalyzer 1.0 software. *Computers and Geosciences*, 32(9), 1420–1431. https://doi.org/10.1016/j.cageo.2006.01.006

Martín, P., García-González, R., Nadal, J., Vergès, J.M. (2016). Perinatal ovicaprine remains and evidence of shepherding activities in Early Holocene enclosure caves: El Mirador (Sierra de Atapuerca, Spain). *Quaternary International* 414, 316-329. http://dx.doi.org/10.1016/j.quaint.2015.08.024

Martín, P., Tornero, C., García, D.C.S., Vergès, J.M. (2021). Early sheep herd management in the inland of the Iberian Peninsula: results of the incremental isotopic analyses of dental remains from El Mirador cave (Sierra de Atapuerca, Spain). *Archaeological and Anthropological Sciences* 13(6), 99 https://doi.org/10.1007/s12520-021-01355-8

Molina-Cardín, A., Campuzano, S. A., Osete, M. L., Rivero-Montero, M., Pavón-Carrasco, F. J., Palencia-Ortas, A., Martín-Hernández, F., Gómez-Paccard, M., Chauvin, A., Guerrero-Suárez, S., Pérez-Fuentes, J.C., McIntosh, G., Catanzariti, G., Sastre Blanco, J.C., Larrazabal, J., Fernández Martínez, V.M., Álvarez Sanchís, J.R., Rodríguez-Hernández, J., Martín Viso, I., Garcia i Rubert, D. (2018). Updated Iberian Archeomagnetic Catalogue: New Full Vector Paleosecular Variation Curve for the Last Three Millennia. *Geochemistry, Geophysics, Geosystems*, 19(10), 3637–3656. https://doi.org/10.1029/2018GC007781

Osete, M. L., Molina-Cardín, A., Campuzano, S. A., Aguilella-Arzo, G., Barrachina-Ibañez, A., Falomir-Granell, F., Oliver Foix, A., Gómez-Paccard, M., Martín-Hernández, F., Palencia-Ortas, A., Pavón-Carrasco, F.J., Rivero-Montero, M. (2020). Two archaeomagnetic intensity maxima and rapid directional variation rates during the Early Iron Age observed at Iberian coordinates. Implications on the evolution of the Levantine Iron Age Anomaly. *Earth and Planetary Science Letters*, 533, 116047. https://doi.org/10.1016/j.epsl.2019.116047

Pavón-Carrasco, F. J., Campuzano, S. A., Rivero-Montero, M., Molina-Cardín, A., Gómez-Paccard, M., Osete, M. L. (2021). SCHA.DIF.4k: 4,000 Years of Paleomagnetic Reconstruction for Europe and Its Application for Dating. *Journal of Geophysical Research: Solid Earth,* 126, e2020JB021237. https://doi.org/10.1029/2020JB021237

Pavón-Carrasco, F. J., Osete, M. L., Torta, J. M., De Santis, A. (2014). A geomagnetic field model for the Holocene based on archaeomagnetic and lava flow data. *Earth and Planetary Science Letters*, 388, 98–109. https://doi.org/10.1016/j.epsl.2013.11.046

Polo-Díaz, A., Alonso-Eguíluz, M., Ruiz, M., Pérez, S., Mujika, J.A., Albert, R.M., Fernández-Eraso, J. (2016). Management of residues and natural resources at San Cristóbal rock-shelter: contribution to the characterization of Chalcolithic agropastoral groups in the Iberian Peninsula . *Quaternary International*, 414, 202–225. https://doi.org/10.1016/j.quaint.2016.02.013

Polo-Díaz, A., Martínez-Moreno, J., Benito-Calvo, A., Mora, R. (2014). Prehistoric herding facilities: site formation processes and archaeological dynamics in Cova Gran de Santa Linya (Southeastern Prepyrenees, Iberia). *Journal of Archaeological Science,* 41, 784–800. https://doi.org/10.1016/j.jas.2013.09.013

Reimer, P. J., Edouard Bard, B., Alex Bayliss, B., Warren Beck, B. J., Paul Blackwell, B. G., Christopher Bronk Ramsey, B. (2013). Intcal13 and Marine13 Radiocarbon Age Calibration Curves 0–50,000 Years Cal Bp. *Radiocarbon*, 55(4), 1869–1887. https://doi.org/10.1017/S0033822200048864

Schnepp, E., Thallner, D., Arneitz, P., Leonhardt, R. (2020). New archeomagnetic secular variation data from Central Europe, II: Intensities. *Physics of the Earth and Planetary Interiors,* 309, 106605. https://doi.org/10.1016/j.pepi.2020.106605

Stacey, F. D. (1967). The Koenigsberger ratio and the nature of thermoremanence in igneous rocks. *Earth and Planetary Science Letters*, 2, 67–68. https://doi.org/10.1016/0012-821X(67)90174-4

Tauxe, L. (2010). *Essentials of Paleomagnetism.* ISBN: 9780520260313

Tema, E., Lanos, P. (2021). New Italian directional and intensity archaeomagnetic reference curves for the past 3000 years: Insights on secular variation and implications on dating. *Archaeometry*, 63 (2), 428-445.

Vergès, J. M., Allué, E., Fontanals, M., Morales, J. I., Martín, P., Carrancho, Á., et al. (2016a). El Mirador cave (Sierra de Atapuerca, Burgos, Spain): A whole perspective. *Quaternary International*, 414, 236–243. https://doi.org/10.1016/j.quaint.2016.01.044

Vergès, J.Mª., Burguet-Coca, A., Allué, E., Expósito, I., Guardiola, M., Martin, P., Morales, I. J., Burjachs, F., Cabanes, D.; Carrancho, Á., Vallverdú, J. (2016b). The Mas del Pepet experimental programme for the study of prehistoric livestock practices: Preliminary data from dung burning. *Quaternary International,* 414, 304–315. https://doi.org/10.1016/j.quaint.2016.01.032

Figure captions

Fig.1 a. Progressive isothermal remanent magnetization acquisition curves (IRM); **b-g.** thermomagnetic curves (temperature vs. induced magnetization) of ashes and carbonaceous facies. Heating (cooling) cycles are shown in red (blue). Sample code and type of facies are also shown

Fig. 2 Orthogonal NRM demagnetization plots of five representative specimens (ashes and carbonaceous facies) from the burning events studied: **a & e***.* AF demagnetized diagrams; **b-d.** Thermal demagnetization plots. Solid/open circles in orthogonal plots represent the projections of vector endpoints onto the horizontal/vertical plane. The initial intensity (NRM), sample code, facies, main demagnetization steps and the normalized demagnetization intensity spectra are shown for each specimen

Fig. 3 Equal area projection of the five new mean archaeomagnetic directions from El Mirador cave and their associated statistical parameters according to Fisher (1953). N = specimens considered for the calculation of the mean direction; N' = total number of demagnetized specimens; Dec. = declination; Inc.

= inclination; α95 = semi angle of confidence at 95% of probability; *k* = precision parameter. Solid/open symbols correspond to downward/upward inclination

Supplementary information 1 Schematic representation of the relative stratigraphical position of the studied combustion episodes. .

Supplementary information 2 Image of the combustion episodes Ci2 and Ci3. (Each sampling hole is ~2 cm in diameter)

Supplementary information 3 Image of one of the profiles where the combustion episodes Ci5, Ci6 and Ci7 were exposed

Supplementary information 4 Information about the sampling process.

Supplementary information 5 Detailed information about the oriented specimens. It is worth mentioning that the category “Ash facies” was assigned macroscopically and has a broad meaning (it corresponds to samples that have ash content, but not necessarily only ash)

Supplementary information 6 Day et al. (1977) plot (logarithmic scale), including the areas of mixtures of single domain (SD) and multidomain (MD) or superparamagnetic (SP) magnetite grains according to Dunlop (2002). (PSD = pseudo-single domain)

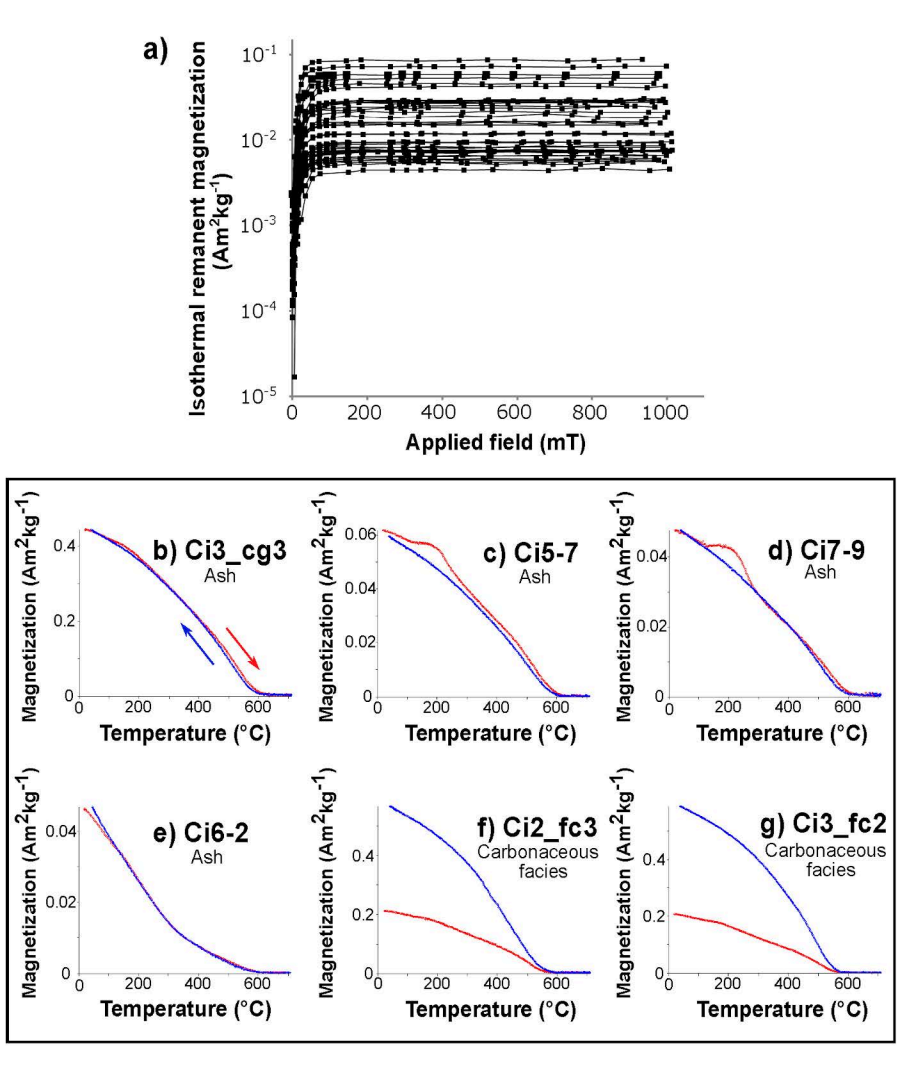
a)
Isothermal remanent magnetization (Am²kg⁻¹)
10⁻¹
10⁻²
10⁻³
10⁻⁴
10⁻⁵
0
200
400
600
800
1000
Applied field (mT)
b) Ci3_cg3
Ash
c) Ci5-7
Ash
d) Ci7-9
Ash
e) Ci6-2
Ash
f) Ci2_fc3
Carbonaceous facies
g) Ci3_fc2
Carbonaceous facies
Magnetization (Am²kg⁻¹)
Temperature (°C)

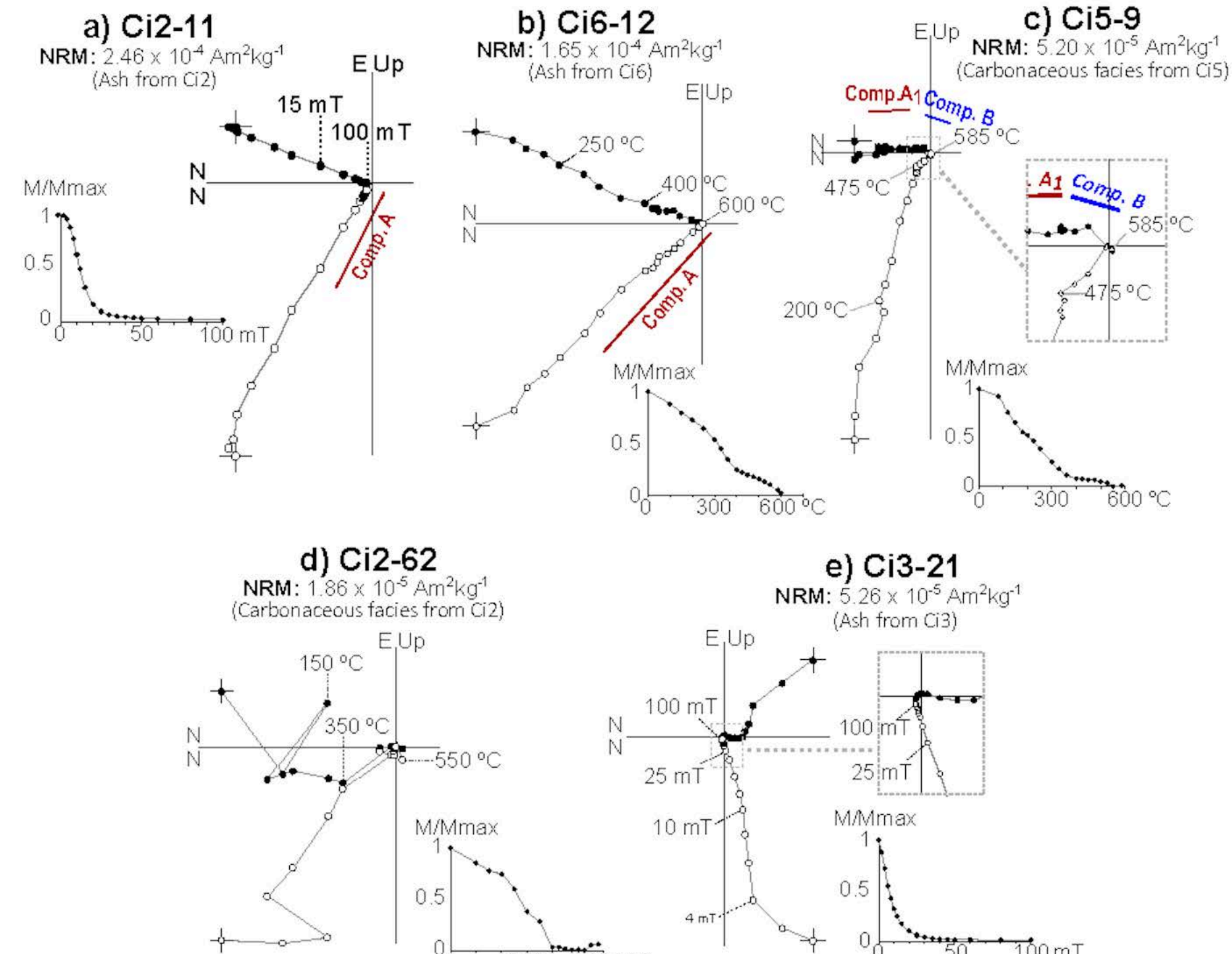
a) Ci2-11
NRM: 2.46 x 10-4 Am2kg-1
(Ash from Ci2)
E Up
15 mT
100 mT
N
N
Comp. A
M/Mmax
1
0.5
0
0
50
100 mT
b) Ci6-12
NRM: 1.65 x 10-4 Am2kg-1
(Ash from Ci6)
E Up
250 °C
400 °C
600 °C
N
N
Comp. A
M/Mmax
1
0.5
0
0
300
600 °C
c) Ci5-9
NRM: 5.20 x 10-5 Am2kg-1
(Carbonaceous facies from Ci5)
E Up
Comp A1
Comp. B
585 °C
N
N
475 °C
200 °C
A1
Comp. B
585 °C
475 °C
M/Mmax
1
0.5
0
0
300
600 °C
d) Ci2-62
NRM: 1.86 x 10-5 Am2kg-1
(Carbonaceous facies from Ci2)
E Up
150 °C
350 °C
550 °C
N
N
M/Mmax
1
0.5
0
0
300
600 °C
e) Ci3-21
NRM: 5.26 x 10-5 Am2kg-1
(Ash from Ci3)
E Up
100 mT
25 mT
10 mT
4 mT
N
N
100 mT
25 mT
M/Mmax
1
0.5
0
0
50
100 mT

a) Ci2

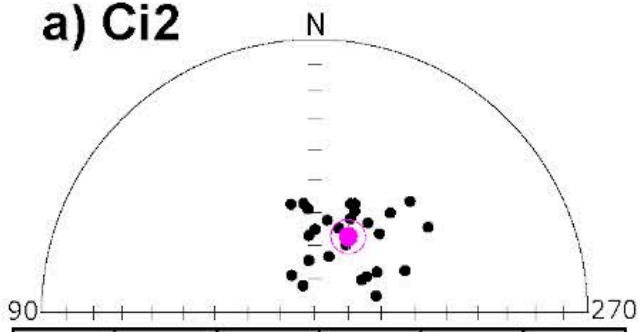

N	N'	Dec (°)	Inc (°)	α95 (°)	*k*
26	42	23.9	65.1	5.1	31.9

b) Ci3

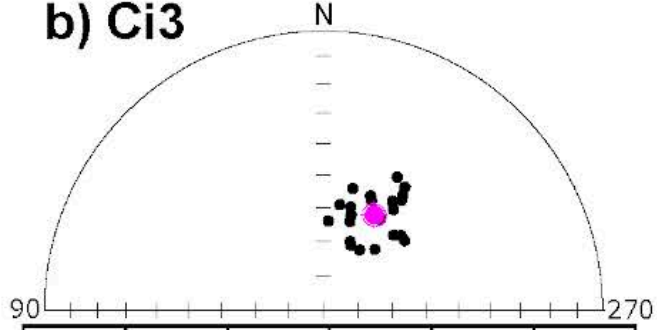

N	N'	Dec (°)	Inc (°)	α95 (°)	*k*
24	41	28.1	58.3	3.4	78.2

c) Ci5

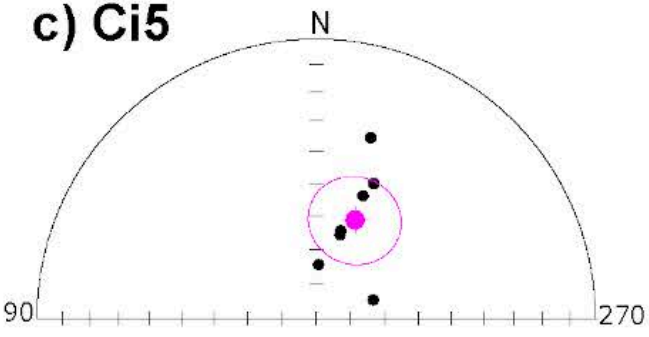

N	N'	Dec (°)	Inc (°)	α95 (°)	*k*
7	16	21.5	58.9	13.2	21.9

d) Ci6

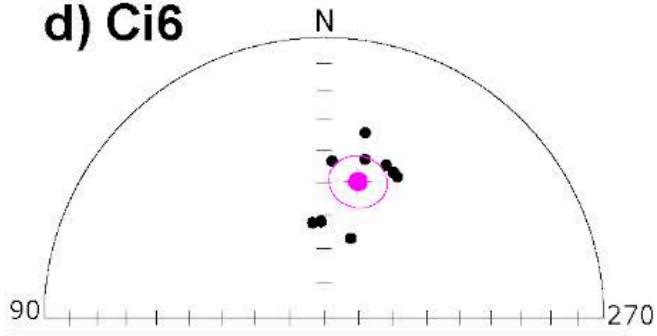

N	N'	Dec (°)	Inc (°)	α95 (°)	*k*
10	16	14.1	48.5	8.0	37.6

e) Ci7

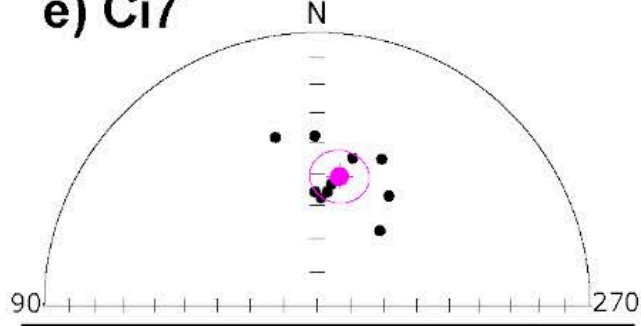

N	N'	Dec (°)	Inc (°)	α95 (°)	*k*
10	12	9.8	50.3	8.3	34.7

Uppermost (most recent)

MIR 104
(1,710-1,510 cal yrs BCE)

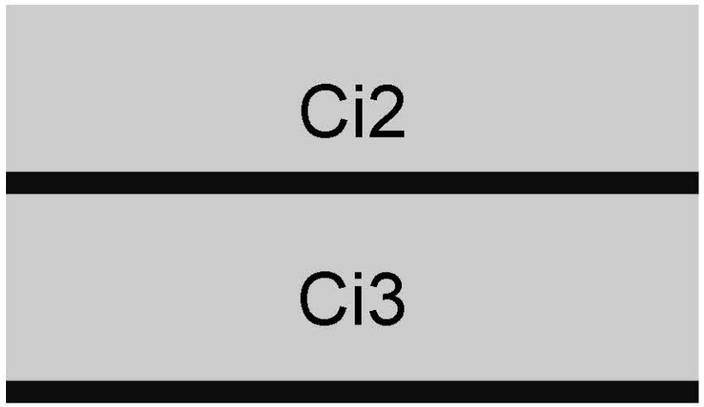

← 30 oriented specimens and 6 bulk samples from Ci2 ash and white ash-like facies

← 12 oriented specimens and 9 bulk samples from Ci2 carbonaceous facies

← 38 oriented specimens and 6 bulk samples from Ci3 ash

← 3 oriented specimens and 3 bulk samples from Ci2 carbonaceous facies

MIR 105

MIR 106

MIR 107
(4,542-4,371 cal yrs BCE)

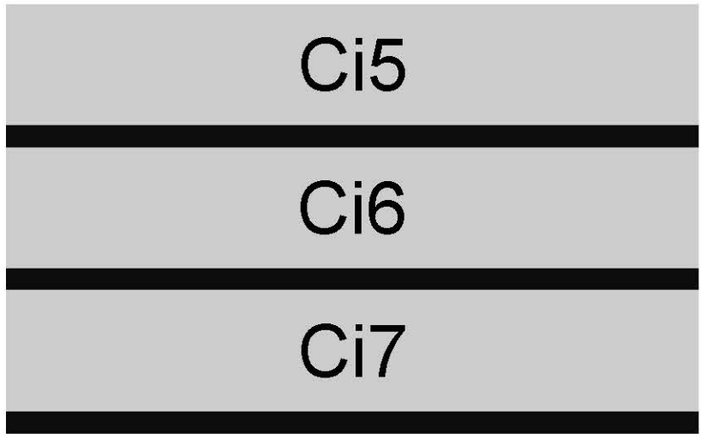

← 12 oriented specimens and 5 bulk samples from Ci5 ash

← 4 oriented specimens from Ci5 carbonaceous facies

← 16 oriented specimens and 8 bulk samples from Ci6 ash

← 12 oriented specimens and 6 bulk samples from Ci7 ash

Lowermost (oldest)


Ci2
Ci3
10 cm

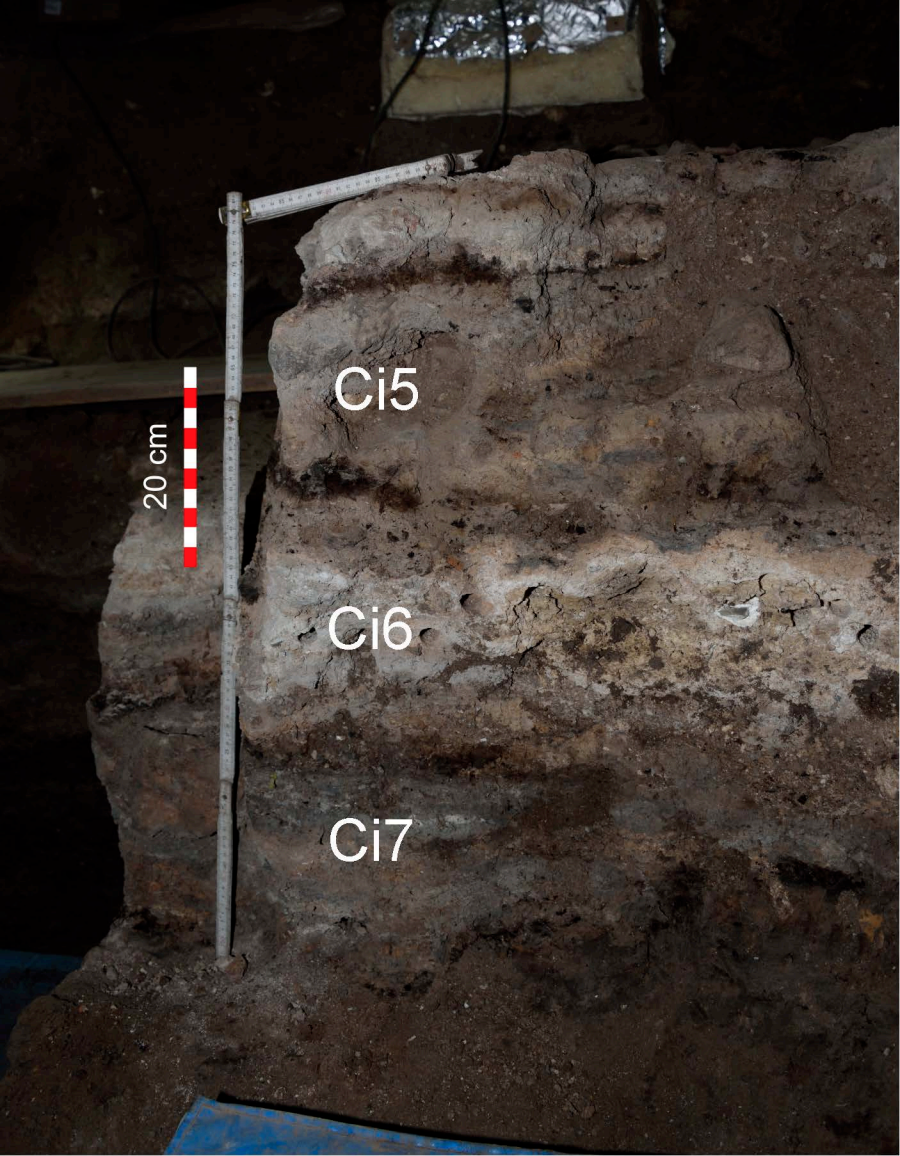
Ci5
Ci6
Ci7
20 cm

Supplementary Information 4. ***Information about the sampling***

A device designed for soft (non-lithified) materials was used to collect oriented samples (**Fig. SI4.1a**). The main parts of the device are a hollow, metallic (non-magnetic) tube; another tube inserted into the metallic one to help to remove the samples (the white piece in the right of **Fig. SI4.1a**); and a plate to place the magnetic compass. The sampling process consists of pressing the metallic tube tube against the profile. Thus, the sample is trapped inside the tube. While the tube is still inside the profile, we get the Azimut of the sample with the help of compass equipped in the device. After that, we remove the tube from the profile. Then, we use the white tube to carefully push the sample out of the metallic tube and to introduce it in a capsule (**Fig. SI4.1b**). The capsules can be made of plastic (left, **Fig. SI4.1b**) or quartz (right, **Fig. SI4.1b**).

No specific device is needed to collect non oriented samples. A few grams of sample (less than 1 g is needed for the rock magnetic analyses performed here) are simply introduced in a plastic bag.

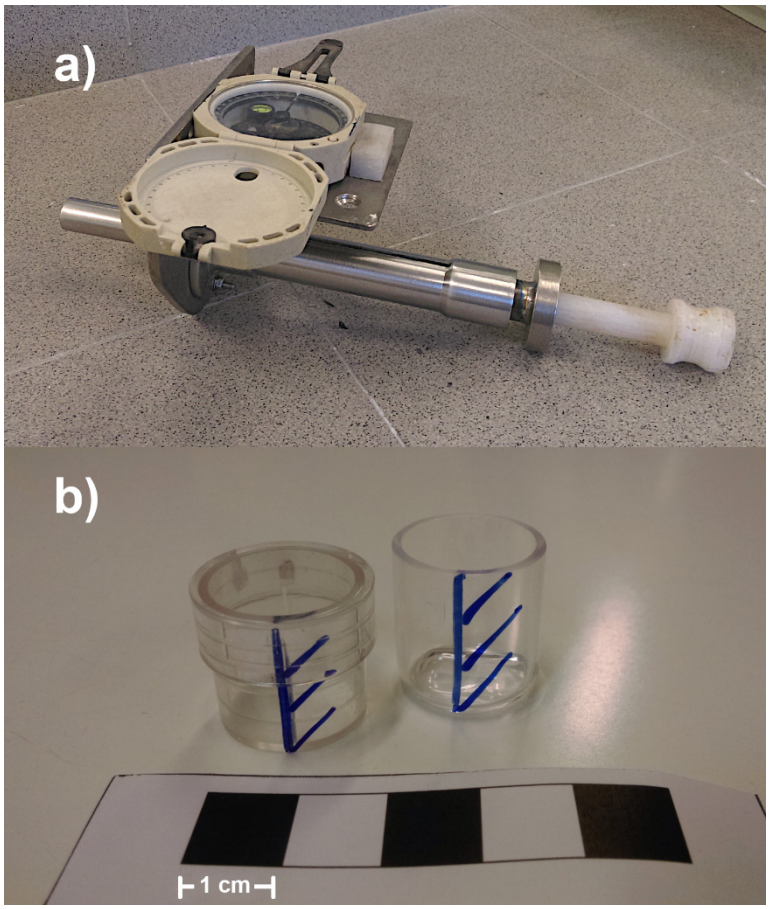

Fig. SI4. 1 a. Sampling device for soft (non-lithified) materials. **b**. Capsules to infroduce the samples (plastic box in the left; quartz box in the right). c. Schematic representation of the sampling process. The device is pressed against the profile and the sample is trapped in the tube.

SPECIMEN	COMBUSTION EPISODE	FACIES	MASS WITHOUT CAPSULE (kg)	NRM (Am^2kg^{-1})	INITIAL SUSCEPTIBILITY (m^3kg^{-1})	Q_n RATIO
Ci2-1	Ci2	Carbonaceous facies	0.0022626	2.04E-05	5.35E-07	1.06
Ci2-2	Ci2	Carbonaceous facies	0.0019886	2.29E-05	5.23E-07	1.21
Ci2-3	Ci2	Carbonaceous facies	0.0020826	2.73E-05	4.17E-07	1.82
Ci2-4	Ci2	Carbonaceous facies	0.0018036	6.87E-05	7.21E-07	2.65
Ci2-5	Ci2	Carbonaceous facies	0.0029606	1.17E-04	6.72E-07	4.82
Ci2-6	Ci2	Carbonaceous facies	0.0024216	7.16E-05	7.23E-07	2.75
Ci2-7	Ci2	Carbonaceous facies	0.0021186	5.49E-05	7.17E-07	2.13
Ci2-8	Ci2	Carbonaceous facies	0.0024846	6.85E-05	7.85E-07	2.43
Ci2-9	Ci2	Ash facies	0.0023536	5.11E-04	4.00E-06	3.55
Ci2-10	Ci2	Ash facies	0.0023866	7.95E-04	3.28E-06	6.73
Ci2-11	Ci2	Ash facies	0.0020006	2.46E-04	1.04E-06	6.59
Ci2-12	Ci2	Ash facies	0.0021316	7.74E-05	3.83E-07	5.61
Ci2-13	Ci2	Ash facies	0.0018676	4.22E-05	5.46E-07	2.15
Ci2-14	Ci2	Ash facies	0.0019336	1.24E-05	3.29E-07	1.05
Ci2-15	Ci2	Ash facies	0.0026446	2.87E-04	1.58E-06	5.03
Ci2-16	Ci2	Ash facies	0.0023216	1.16E-04	7.62E-07	4.24
Ci2-17	Ci2	Ash facies	0.0025356	2.69E-05	2.72E-07	2.75
Ci2-18	Ci2	Ash facies	0.0022646	2.44E-04	2.01E-06	3.37
Ci2-19	Ci2	Ash facies	0.0024946	3.67E-04	2.74E-06	3.73
Ci2-20	Ci2	Ash facies	0.0022766	7.24E-05	1.43E-06	1.41
Ci2-21	Ci2	Ash facies	0.0025966	3.66E-04	2.89E-06	3.52
Ci2-22	Ci2	Ash facies	0.0024426	4.41E-04	1.96E-06	6.24
Ci2-23	Ci2	Ash facies	0.0022016	3.66E-04	1.99E-06	5.13
Ci2-24	Ci2	Ash facies	0.0020116	2.54E-04	3.59E-06	1.96
Ci2-25	Ci2	Ash facies	0.0019906	3.52E-04	4.44E-06	2.20
Ci2-26	Ci2	Ash facies	0.0021566	1.95E-04	1.48E-06	3.64
Ci2-27	Ci2	Ash facies	0.0021416	9.12E-04	3.61E-06	7.03
Ci2-28	Ci2	Ash facies	0.0022416	3.04E-04	1.97E-06	4.28
Ci2-29	Ci2	Ash facies	0.0022226	3.96E-04	4.06E-06	2.71
Ci2-50	Ci2	Ash facies	0.0018666	3.25E-04	2.94E-06	3.07
Ci2-51	Ci2	Ash facies	0.0019086			
Ci2-52	Ci2	Ash facies	0.0015476	2.22E-04	2.82E-06	2.19
Ci2-53	Ci2	Ash facies	0.0018246	2.27E-04	2.79E-06	2.26
Ci2-54	Ci2	White facies	0.0021436	5.68E-05	6.86E-07	2.30
Ci2-55	Ci2	Ash facies	0.0022066	3.82E-04	3.57E-06	2.97
Ci2-56	Ci2	White facies	0.0025093	3.17E-05	4.03E-07	2.19
Ci2-57	Ci2	White facies	0.0030323	9.10E-06	6.40E-08	3.96
Ci2-58	Ci2	Ash facies	0.0022836	6.31E-04	2.14E-06	8.20
Ci2-59	Ci2	Carbonaceous facies	0.0028886	4.76E-05	5.47E-07	2.42
Ci2-60	Ci2	Carbonaceous facies	0.0024293	9.46E-05	7.37E-07	3.57
Ci2-61	Ci2	Carbonaceous facies	0.0028703	2.93E-05	4.60E-07	1.77
Ci2-62	Ci2	Carbonaceous facies	0.0027313	1.86E-05	1.90E-07	2.72
Ci3-1	Ci3	Ash facies	0.0026016	7.84E-05	9.26E-07	2.35
Ci3-2	Ci3	Ash facies	0.0023796	1.50E-04	1.51E-06	2.75
Ci3-3	Ci3	Ash facies	0.0024496	2.70E-04	1.56E-06	4.82
Ci3-4	Ci3	Ash facies	0.0025566	9.07E-05	7.47E-07	3.37
Ci3-5	Ci3	Ash facies	0.0022766	1.79E-04	1.34E-06	3.72
Ci3-6	Ci3	Ash facies	0.0025806	1.12E-04	9.07E-07	3.43
Ci3-7	Ci3	Ash facies	0.0022786	1.14E-04	1.42E-06	2.23
Ci3-8	Ci3	Ash facies	0.0021936	1.10E-04	9.25E-07	3.30
Ci3-9	Ci3	Ash facies	0.0026596	2.17E-04	9.59E-07	6.29
Ci3-10	Ci3	Ash facies	0.0024986	1.08E-04	6.72E-07	4.47
Ci3-11	Ci3	Ash facies	0.0027036	9.99E-05	6.99E-07	3.97
Ci3-12	Ci3	Ash facies	0.0023516	1.34E-04	9.74E-07	3.82
Ci3-13	Ci3	Ash facies	0.0025156	1.50E-04	8.31E-07	5.00
Ci3-14	Ci3	Ash facies	0.0019646	9.48E-05	1.77E-06	1.49

Ci3-15	Ci3	Ash facies	0.0020286	2.02E-04	1.72E-06	3.26
Ci3-16	Ci3	Ash facies	0.0025586	3.55E-04	2.61E-06	3.78
Ci3-17	Ci3	Ash facies	0.0025046	4.12E-04	3.27E-06	3.50
Ci3-18	Ci3	Ash facies	0.0024386	6.33E-04	3.72E-06	4.72
Ci3-19	Ci3	Ash facies	0.0020916	2.00E-04	1.53E-06	3.63
Ci3-20	Ci3	Ash facies	0.0027086	2.48E-04	3.03E-06	2.27
Ci3-21	Ci3	Ash facies	0.0026606	5.26E-05	1.39E-06	1.05
Ci3-22	Ci3	Ash facies	0.0027906	4.55E-05	1.64E-06	0.77
Ci3-23	Ci3	Ash facies	0.0028056	4.87E-05	1.83E-06	0.74
Ci3-40	Ci3	Ash facies	0.0024656	8.73E-05	6.41E-07	3.79
Ci3-41	Ci3	Ash facies	0.0025016	2.83E-04	1.46E-06	5.39
Ci3-42	Ci3	Ash facies	0.0027096	2.96E-04	1.32E-06	6.22
Ci3-43	Ci3	Ash facies	0.0026536	5.08E-04	2.83E-06	5.00
Ci3-44	Ci3	Ash facies	0.0028606	8.68E-05	1.64E-06	1.47
Ci3-45	Ci3	Ash facies	0.0028766	8.83E-05	1.98E-06	1.24
Ci3-46	Ci3	Ash facies	0.0028026	2.20E-04	8.85E-07	6.92
Ci3-47	Ci3	Ash facies	0.0034953	1.81E-04	7.81E-07	6.44
Ci3-48	Ci3	Ash facies	0.0029556	1.66E-04	1.11E-06	4.15
Ci3-49	Ci3	Ash facies	0.0028453	7.80E-05	8.33E-07	2.60
Ci3-50	Ci3	Ash facies	0.0028713	8.18E-05	7.52E-07	3.02
Ci3-51	Ci3	Ash facies	0.0024406	7.20E-05	6.97E-07	2.87
Ci3-52	Ci3	Ash facies and carbonaceous facies	0.0020866	1.26E-04	1.12E-06	3.12
Ci3-53	Ci3	Ash facies	0.0027526	1.46E-04	1.12E-06	3.63
Ci3-54	Ci3	Ash facies	0.0029406	2.56E-04	1.49E-06	4.77
Ci3-55	Ci3	Carbonaceous facies	0.0026723	9.30E-05	1.09E-06	2.38
Ci3-56	Ci3	Carbonaceous facies	0.0032763	8.70E-05	1.01E-06	2.39
Ci3-57	Ci3	Carbonaceous facies	0.0027746	6.18E-05	1.16E-06	1.48
Ci5-1	Ci5	Ash facies	0.0030206	6.43E-05	8.61E-07	2.07
Ci5-2	Ci5	Ash facies	0.0020786	5.82E-05	7.26E-07	2.22
Ci5-3	Ci5	Ash facies	0.0028606	8.60E-05	1.10E-06	2.17
Ci5-4	Ci5	Ash facies	0.0023566	1.55E-04	1.57E-06	2.75
Ci5-5	Ci5	Ash facies	0.0027686	1.77E-04	1.34E-06	3.68
Ci5-6	Ci5	Ash facies	0.0022916	1.56E-04	1.43E-06	3.03
Ci5-7	Ci5	Ash facies	0.0043873	7.13E-05	8.78E-07	2.26
Ci5-8	Ci5	Ash facies (may include other surrounding materials)	0.0030626	1.41E-04	2.33E-06	1.68
Ci5-9	Ci5	Carbonaceous facies	0.0045563	5.20E-05	8.78E-07	1.65
Ci5-10	Ci5	Carbonaceous facies	0.0038803	3.64E-05	1.06E-06	0.95
Ci5-11	Ci5	Carbonaceous facies	0.0038783	4.42E-05	8.66E-07	1.42
Ci5-12	Ci5	Ash facies	0.0019826	2.96E-04	2.92E-06	2.81
Ci5-13	Ci5	Ash facies	0.0026876	2.24E-04	2.38E-06	2.61
Ci5-14	Ci5	Ash facies	0.0027226	2.59E-04	2.15E-06	3.35
Ci5-15	Ci5	Ash facies	0.0017363	4.89E-04	2.06E-06	6.61
Ci5-16	Ci5	Carbonaceous facies	0.0052266	3.73E-05	1.43E-06	0.72
Ci6-1	Ci6	Ash facies	0.0020246	3.37E-04	1.89E-06	4.95
Ci6-2	Ci6	Ash facies	0.0019506	1.56E-04	1.78E-06	2.43
Ci6-3	Ci6	Ash facies	0.0018386	2.33E-04	2.00E-06	3.23
Ci6-4	Ci6	Ash facies	0.0022853	1.61E-04	1.44E-06	3.10
Ci6-5	Ci6	Ash facies	0.0026423	6.46E-05	9.92E-07	1.81
Ci6-6	Ci6	Ash facies (may include other surrounding materials)	0.0023536	1.95E-04	1.76E-06	3.08
Ci6-7	Ci6	Ash facies	0.0017646	7.88E-05	1.15E-06	1.90
Ci6-8	Ci6	Ash facies	0.0030973	1.10E-04	1.41E-06	2.16
Ci6-9	Ci6	Ash facies	0.0024566	1.54E-04	1.99E-06	2.16
Ci6-10	Ci6	Ash facies	0.0030276	9.42E-05	8.59E-07	3.05
Ci6-11	Ci6	Ash facies	0.0024806	1.17E-04	1.58E-06	2.05

Ci6-12	Ci6	Ash facies	0.0029493	1.65E-04	1.81E-06	2.53
Ci6-13	Ci6	Ash facies (may include other surrounding materials)	0.0023156	1.35E-04	1.31E-06	2.86
Ci6-14	Ci6	Ash facies (may include other surrounding materials)	0.0024566	1.23E-04	1.19E-06	2.88
Ci6-15	Ci6	Ash facies (may include other surrounding materials)	0.0027856	1.37E-04	1.48E-06	2.56
Ci6-16	Ci6	Ash facies	0.0032506	1.80E-04	1.99E-06	2.52
Ci7-1	Ci7	Ash facies	0.0028056	7.57E-05	9.30E-07	2.26
Ci7-2	Ci7	Ash facies	0.0028216	8.52E-05	1.07E-06	2.20
Ci7-3	Ci7	Ash facies	0.0028656	1.38E-04	1.29E-06	2.97
Ci7-4	Ci7	Ash facies	0.0031456	1.72E-04	1.49E-06	3.20
Ci7-5	Ci7	Ash facies	0.0030786	1.07E-04	1.10E-06	2.70
Ci7-6	Ci7	Ash facies	0.0026706	9.54E-05	1.36E-06	1.95
Ci7-7	Ci7	Ash facies	0.0033016	1.30E-04	1.38E-06	2.62
Ci7-8	Ci7	Ash facies	0.0029186	1.86E-04	1.60E-06	3.23
Ci7-9	Ci7	Ash facies	0.0027946	9.72E-05	1.68E-06	1.61
Ci7-10	Ci7	Ash facies	0.0043413	2.64E-05	9.40E-07	0.78
Ci7-11	Ci7	Ash facies	0.0043343	2.76E-05	5.91E-07	1.30
Ci7-12	Ci7	Ash facies	0.0036196	5.06E-05	1.17E-06	1.20

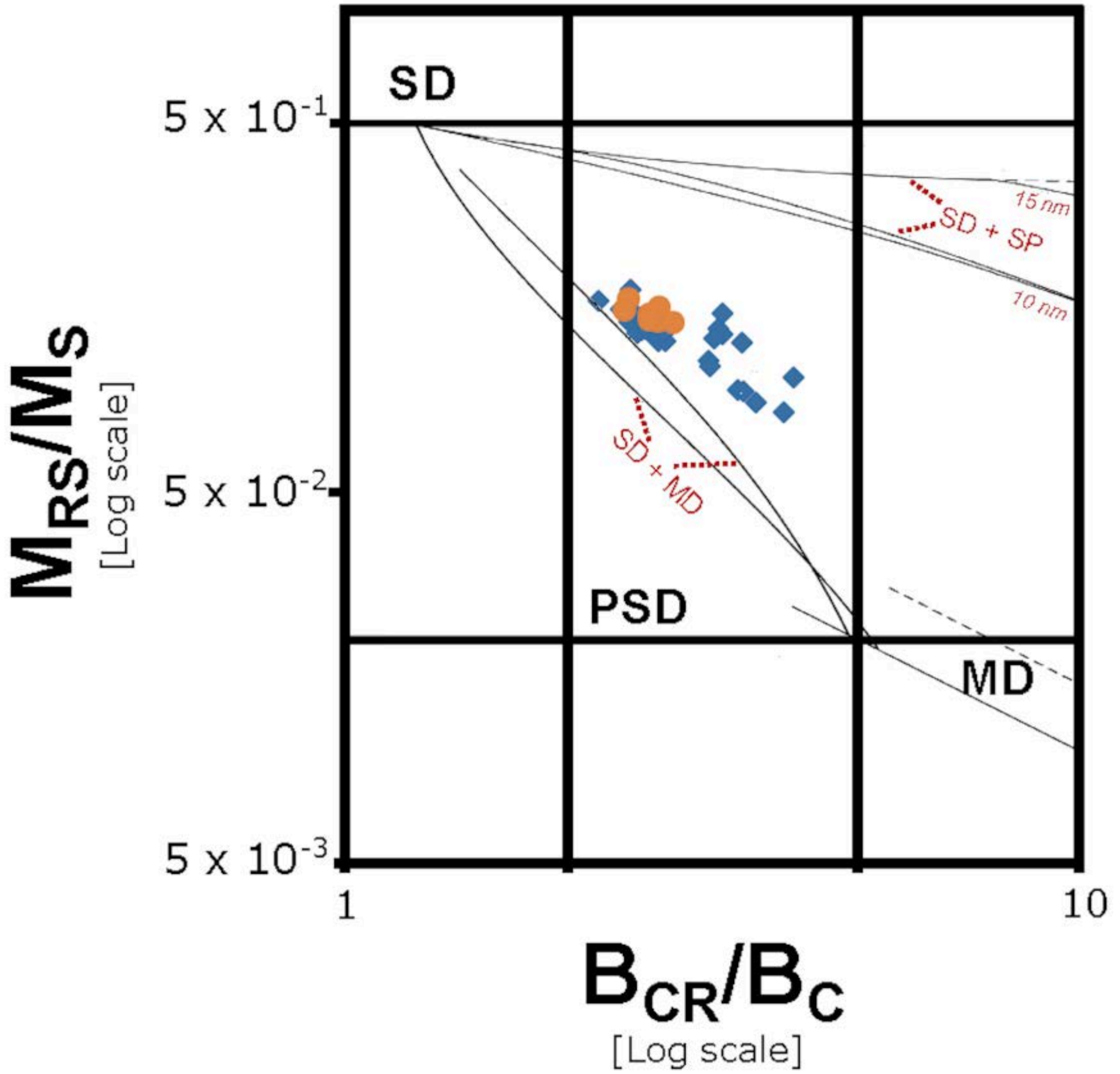
SD
PSD
MD
5 x 10-1
5 x 10-2
5 x 10-3
1
10
MRS/MS
[Log scale]
BCR/BC
[Log scale]
15 nm
SD + SP
10 nm
SD + MD